13

Calculation and optimization of the limiting characteristics of a single-channel dual-spectrum image receiver of objects emitting in the ultraviolet range

© P.A. Zolotukhin, E.A. Il'ichev, G.N. Petrukhin, A.V. Popov, G.S. Rychkov, E.G. Teverovskaya

National Research University of Electronic Technology (MIET),
124498 Zelenograd, Russia
e-mail: edil44@mail.ru, alexcoretex@gmail.com

Received April 12, 2022
Revised April 12, 2022
Accepted May 18, 2022

A single-channel, two-spectral image receiver of objects emitting in UV radiation, made in the image intensifier tube architecture, was proposed and investigated. With the help of the COMSOL Multiphysics software package, search optimal measurements of the potential on the elements of the image receiver (silicon membrane, germanium and diamond photocathode, MCP input and output sensors) were implemented, which provides the possibility of registering and presence of UV objects in relation to the terrain.

Keywords: image intensifier tube, diamond photocathode, germanium photocathode, ultraviolet radiation, object imager, photoelectron emission, secondary electron emission.

DOI: 10.21883/TP.2022.09.54691.97-22

Introduction

At present, the request for the development of a single-channel dual-spectrum image receiver of objects emitting in the ultraviolet range (hereinafter referred to as the UV object, spectral sensitivity range 180−255 nm) in relation to the surrounding area is relevant. The formation of images of the UV object and the surrounding area is carried out by a single optical system of lens based on BaF_2, the focal planes of which, with images of the UV object and the surrounding area, are separated in space by a distance of ~ 1 mm. Diamond and germanium photocathodes, respectively, are placed in the focal planes of the lens. A diamond photocathode records an image of the object emitting in the UV range ($0.18-0.25\,\mu$m) [1,2], and an image of the surrounding area is recorded in the reflected radiation of the night sky in the near infrared (IR) range ($0.8-1.5\,\mu$m). The proposed image receiver can be used in solving a wide range of problems. They include: non-contact monitoring of the technical condition of high-voltage electric power facilities for the purpose of early detection of technical malfunctions of high-voltage equipment (by registering „partial" and „corona" discharges); diagnostics of the state of contact circuits of transformer substations and contact networks of railways; noncontact monitoring of territories contaminated with radioactive substances.

The proposed design of a single-channel dual-spectrum image receiver of UV objects, made based on the image intensifier tube (IIT) architecture, is shown in Fig. 1.

The said receiver integrates a sequence of a set of physical effects and procedures. Among them: the formation by the optical system of the images of a UV object and the surrounding area in the plane of the diamond and germanium photocathodes, respectively; conversion of optical images of the UV object and the surrounding area into images in electron flows; amplification of the aggregate image in electron flows, carrying information about the object and its surrounding area, executed in a microchannel plate (MCP) through the effect of secondary emission of electrons; converting the images pattern in the electron flow into images pattern of the visible part of the optical range by means of cathodoluminescence.

The object image (180−255 nm) is projected by a system of BaF_2 lens into the plane of the diamond photocathode, absorbed by its substance, and in proportion to the radiation intensity is converted into the image in photoelectrons. The image of the area surrounding the UV object, formed in the reflected IR radiation of the night sky ($0.8-1.55\,\mu$m), is projected by the BaF_2 lens system, but by this time into the plane of the germanium photocathode, is absorbed by its substance and, proportionally to the intensity of IR radiation is converted into the image in photoelectrons. Space diversity of the focal planes of images of objects emitting in the UV range and of images of the surrounding area is provided by the geometry of the lens and the difference in the refractive indices of their substance (BaF_2) in relation to the specified (IR and UV) spectral ranges of detected radiation. This makes it possible to separate their focal planes in space by distances ~ 1 mm practically convenient for the device implementation. Thus, the optical images of the UV object and the area surrounding the UV object are converted into images in photoelectrons, the superposition of the flows of which is read in the

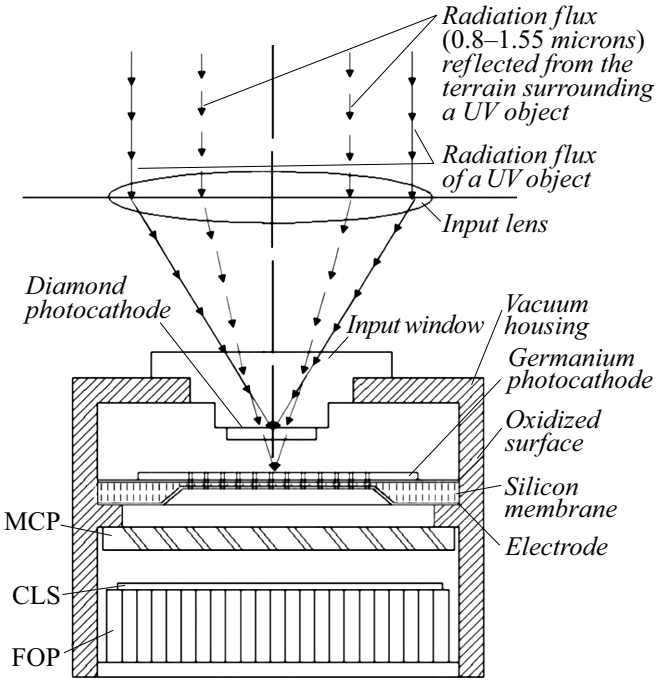

Figure 1. Schematic representation of the design of single-channel dual-spectrum receiver for images of UV objects in relation to the surrounding area, made in EOC architecture.

direction of the MCP, through coaxially located holes in the germanium photocathode and in the silicon membrane. The resulting image in the electron flows is amplified by the MCP due to the effect of secondary emission of the electrons, accelerated in the vacuum gap by the potential difference field between the MCP output electrode and the cathodoluminescent screen (CLS), and then projected onto the CLE. Images of UV object against the background of the surrounding area, entering the CLS in the form of an amplified electrons flow are proportionally converted into images in the photon flows of the visible part of the optical range. The resultant images are output from the device housing by means of a fiber optic plate (FOP) and can be read both visually, and by means of a charge coupled device (CCD) of the receiver, the output window of which is connected to the FOP by the immersion medium.

The efficiency of the discussed single-channel dual-spectrum innovative receiver for images of objects emitting in the UV range in relation to the image of the surrounding area will be determined by the quality of integration in the device of the listed physical effects and the optimal choice of control potentials on its basic elements.

1. Model representations and calculation results

The analysis of the nature and degree of influence of design features and power supply modes on the efficiency of the device is necessary to select and to match the potentials of photocathodes and the reading unit (silicon membrane and MCP input electrode) of the image receiver. In the process of analysis and calculations we used the prominent functional dependences and physical concepts developed in studies of the above physical effects.

When calculating the intensity of electric fields affecting the photoelectron stream, equation (1) was used, which describes the relationship between electric fields and potentials:

$$\mathbf{E} = -\nabla\phi, \tag{1}$$

where $\mathbf{E}$ is superposition of electric fields:

$$\mathbf{E} = \mathbf{E}_{DPh} + \mathbf{E}_{GPh} + \mathbf{E}_{\mathrm{Si}} + \mathbf{E}_{\mathrm{MCP}} + \mathbf{E}_{coulomb}. \tag{2}$$

Here $\mathbf{E}_{DPh}$ is the electric field strength vs. the potential of the diamond photocathode, $\mathbf{E}_{GPh}$ is the electric field strength vs. the potential of the germanium photocathode, $\mathbf{E}_{\mathrm{Si}}$ is the electric field strength vs. silicon membrane potential, $\mathbf{E}_{\mathrm{MCP}}$ is the electric field strength vs. the potential of the MCP input electrode, $\mathbf{E}_{coulomb}$ is the electric field strength associated with the Coulomb interaction of electrons with each other. The latter is described by the expression

$$\mathbf{E}_{coulomb} = \frac{1}{2}\sum_{i,j}^{n}\mathbf{E}_{ij} = \frac{1}{2}\frac{1}{q}\sum_{i,j}^{n} k\,\frac{q_i q_j}{r_{ij}^3}\,\mathbf{r}_{ij}, \tag{3}$$

where $\mathbf{E}_{ij}$ is electric field between i and jth electron, q_i and q_j are charge of i and j electron, k is the Coulomb coefficient, $\mathbf{r}_{ij}$ is radius vector between i and jth electron; summation occurs over each i and j element, while $i \neq j$ and $\mathbf{E}_{ij} = \mathbf{E}_{ji}$.

To describe the refraction of electric fields at the interface of two media in an MCP with permittivity ε_1 and ε_2, equation was used

$$\frac{\mathrm{tg}\,\alpha_1}{\mathrm{tg}\,\alpha_2} = \frac{\varepsilon_1}{\varepsilon_2}, \tag{4}$$

where α_1 and α_2 are the angles between the plane normal of the interface of two media and the electric-field vector located in the medium with permittivity ε_1 and ε_2, respectively.

To describe the influence of the electric field on the photoelectron stream trajectory, equation (5) is used:

$$q\mathbf{E} = m_e\frac{d\mathbf{v}}{dt}, \tag{5}$$

where q is elementary charge, m_e is electron mass and v is electron velocity.

When calculating the multiplication factor of the electron stream in the MCP, expression (6) was used, which ensures the possibility to estimate of the number of produced (in one cycle) secondary electrons during the interaction of primary electrons with the substance of the MCP:

$$n_{secondary} = \frac{E_{primary}}{E_{pair\ form}}, \tag{6}$$

where $E_{primary}$ is the energy of „primary“ electron in each cycle of interactions in the MCP channel,

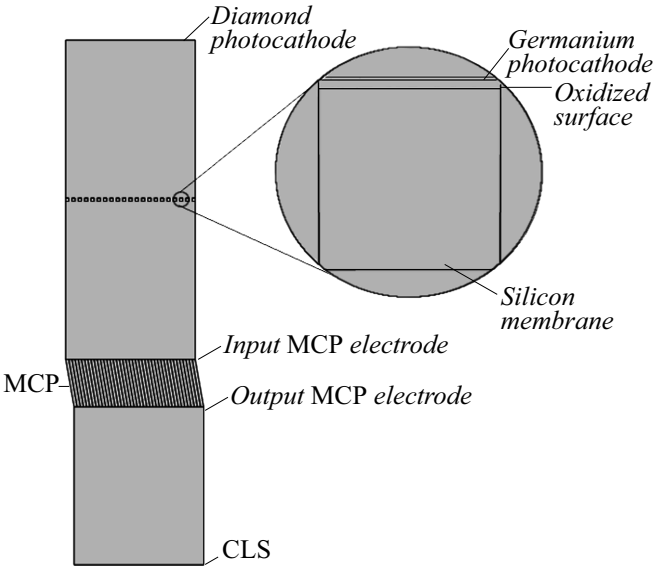

Figure 2. Schematic representation of the reading unit of single-channel dual-spectrum receiver for objects emitting in UV range in relation to the surrounding area.

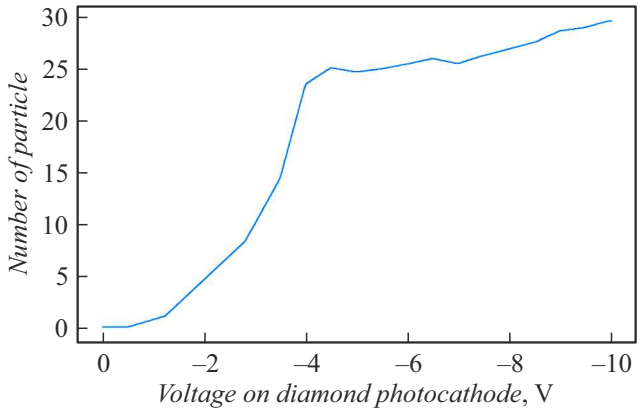

Figure 3. Influence of the photocathode electric potential on the average number of photoelectrons that reached MCP and projected into the raster of any of the holes of its channels.

$E_{pair\ form}$ is the energy of formation of a non-equilibrium pair electron−hole.

When analyzing the processes of specific energy loss by electrons during the reverse transformation of formed in IIT images in electron streams into images in the visible part of the optical range, the Bethe equation is used (functional dependence of specific energy loss by the ionization mechanism during the interaction of light high-energy particles with matter) [3,4].

The integration of the sequence of the listed above physical effects allows to form model representations and study the processes of image transformations and readings, in the basic nodes and in general in a single-channel dual-spectrum receiver of object images in relation to the image of the area surrounding the UV object.

In the present paper a theoretical analysis and numerical calculations were made for the control potentials necessary for the implementation of the process of correct reading the information about the UV object and its surrounding area. A stationary problem (i.e., a situation with stationary electron streams) is discussed. The object of studies and analysis is UV image receiver consisting of the following basic units: diamond photocathode (spectral sensitivity range 180−255 nm); a germanium photocathode (spectral sensitivity range $0.8-1.55\,\mu$m) located on the oxidized surface of the membrane of a thinned silicon wafer; microchannel plate (MCP); CLS (Fig. 2).

1.1. Potential optimization on diamond photocathode

When optimizing the value of the control potential on the diamond photocathode, it is necessary to ensure the energy balance between two photoelectron flows: the electron stream that carries information about the UV object, and the electron stream that carries information about the area surrounding the object. The required energy balance of electron flows is formed by the potentials at the photocathodes, at the thinned silicon membrane with the surface coated with SiO_2, carrying the germanium photocathode, and at the input electrode of the MCP. Their combination should ensure efficient reading of the pattern of images of the object and the area in overlaying of electron flows through coaxial holes in germanium photocathode and the mentioned carrying silicon membrane.

At the potential on the MCP input electrode ~ 300 V, the potential on the thinned silicon membrane ~ 1 V, its thickness $\sim 35\,\mu$m and the potential on the germanium photocathode -0.45 V the dependence on the potential on the diamond photocathode of the average number of photoelectrons reaching the MCP and projected into the raster of holes of any of its channels (Fig. 3) is calculated (and shown below, in the form of a graph).

The functional dependence presented above allows to choose the optimum value of the control potential on the diamond photocathode; this value is in the range of $(-4)-(-5)$ V. Further increasing of the negative potential on the electrode of the diamond photocathode leads to the decreasing of the average number of photoelectrons reaching MCP and projected into the raster of holes of any of its channels.

1.2. Improvement of the potential on the silicon membrane

The positive potential of the silicon membrane ensures the passage of the overlaying of information streams of photoelectrons through coaxial holes in the silicon carrying membrane and in the germanium photocathode. The search for the optimal potential on the silicon membrane is associated with the search for the balance of fields

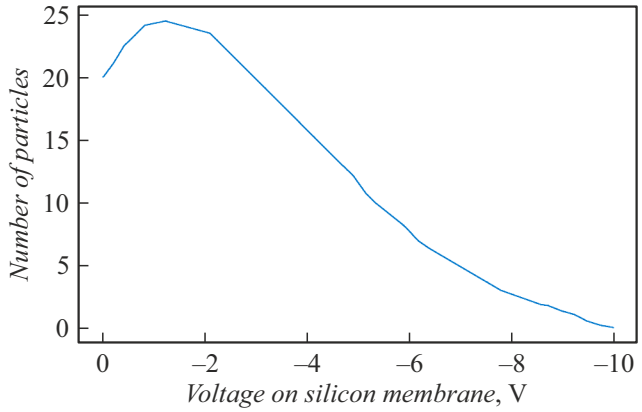

Figure 4. Average number of photoelectrons that reached MCP and projected into the raster of any of the holes of its channels vs. potential on silicon membrane.

from the potentials on the mentioned elements, which ensure the passage of photoelectron flows with minimum losses into coaxially located holes in the silicon membrane and in the germanium photocathode. Fig. 4 shows the dependence of the average number of photoelectrons projected into the raster of each MCP channel on the electric potential of the silicon membrane. In calculations the potential on the diamond photocathode was chosen to be −4.5 V, taking into account the results presented in Fig. 3.

The information presented in Fig. 4 shows that the optimal value of the potential on the silicon membrane is in the range of 1.5−2.0 V, which corresponds to the extremum of the functional dependence of the number of photoelectrons that have passed through the holes in the silicon membrane. The presence of the extremum in this functional dependence is due to the fact that in the specified voltage range, with a given geometry, the balance of electric fields is realized, which ensures the formation of photoelectron trajectories collinear with the symmetry axes of the membrane channels. At potentials below 1.5 V the strength of the electric potential field is insufficient to direct and to „draw“ the dominant number of electrons in the flow through holes in the germanium photocathode and silicon membrane. On the contrary, at potentials above 2 V the average number of photoelectrons reaching the MCP input electrode decreases monotonically with voltage increasing, which is associated with the noncollinearity of the photoelectron trajectories with the symmetry axes of the membrane channels and, as a consequence, with the recombination of photoelectrons on the walls of the channels of the silicon membrane.

Figs. 5 and 6 show patterns of photoelectron trajectories and potential distributions in the space between diamond and germanium photocathodes, at different values of electric potentials on the silicon membrane.

The presented results make it possible to trace the features of the movements and interactions of electron flows and to choose the optimal modes for the formation of electron trajectories in the overlaying of streams.

The average number of photoelectrons captured by the silicon membrane (recombination losses) is estimated for various electric potentials. The results are presented in the form of graphs (Fig. 7).

There is a correlation of the obtained (Fig. 7) results with the information presented earlier in Fig. 4. Thus, an excessive potential increasing on the silicon membrane leads

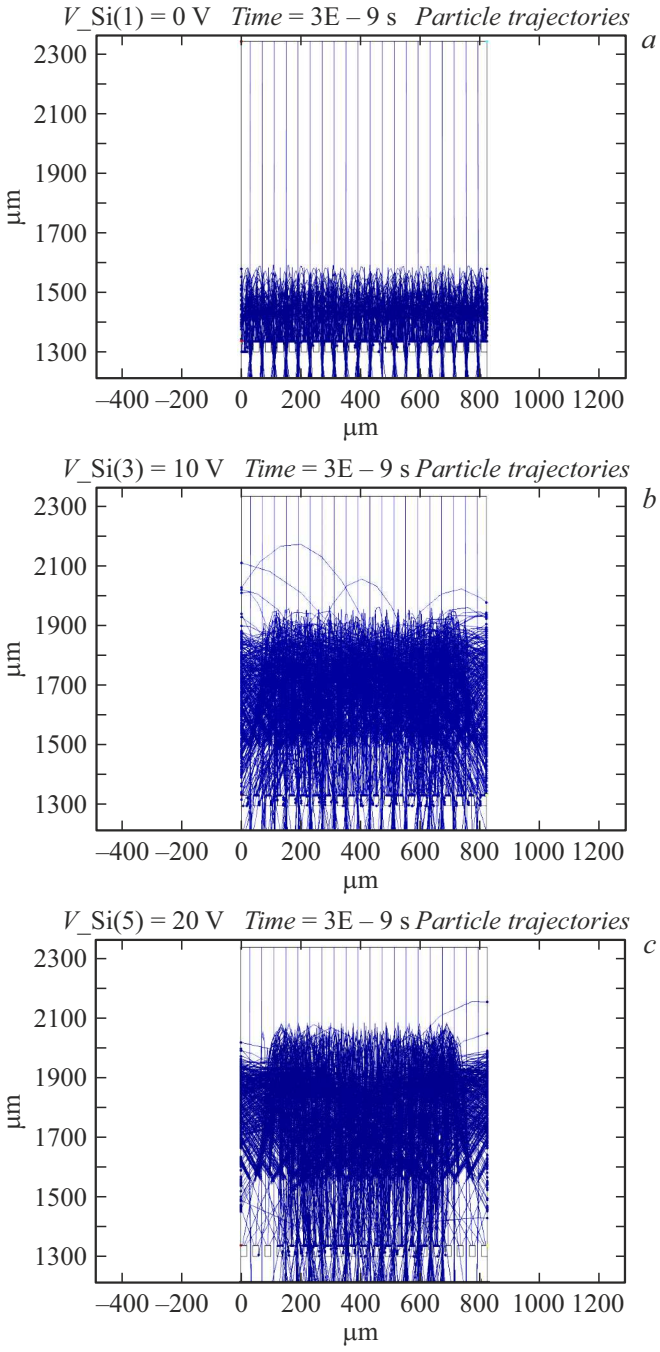

Figure 5. Trajectories of electrons in the space between the diamond photocathode and the silicon membrane at different potentials on the silicon membrane: *a* — 0, *b* — 10, *c* — 20 V.

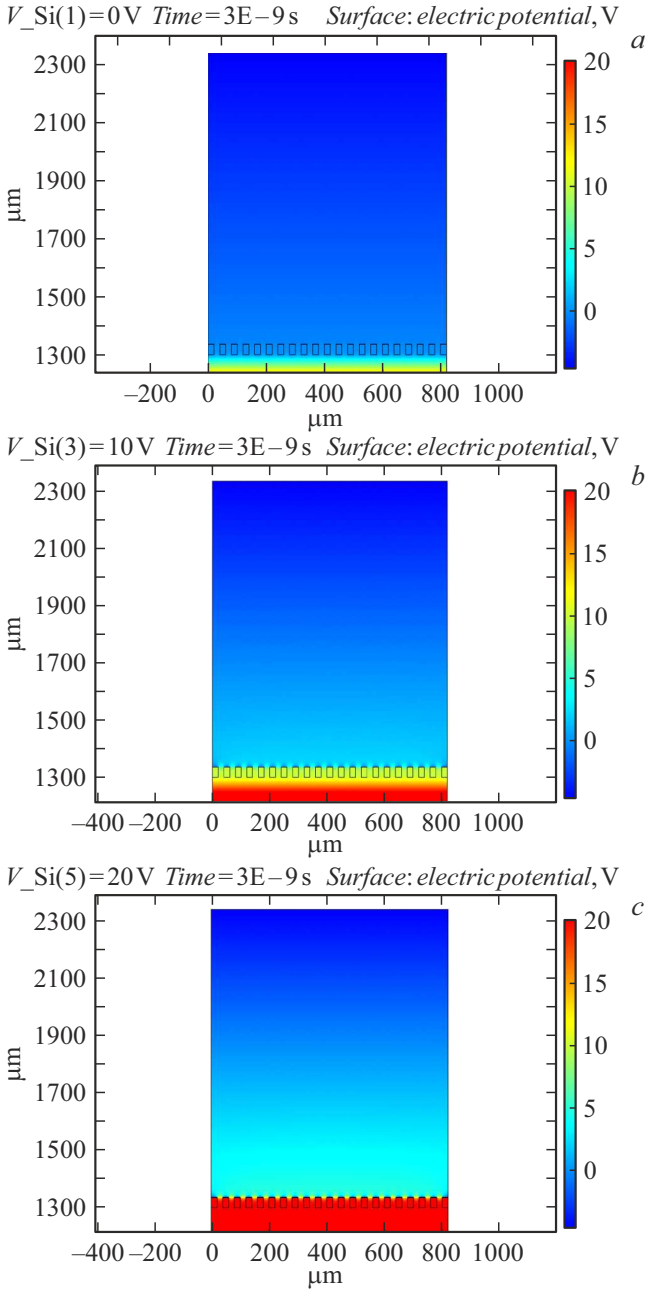

Figure 6. Potential distribution in the space between the diamond photocathode and the silicon membrane at different potential values on the silicon membrane: *a* — 0, *b* — 10, *c* — 20 V.

to the increased loss of electrons in the total photoelectron streams (their recombination on the channel walls).

1.3. Potential optimization at MCP input electrode

When choosing the potential value on the MCP electrodes, the following affecting factors should be taken into account. The potential difference increasing between the input and output electrodes of MCP determines the total multiplication factor of MPC of the electrons flow (determines the internal gain of the device), but is limited by the electrical intensity limit of the MCP substance. Besides, the selection of value of the electrical potential at the MCP input electrode shall significantly exceed the ratio $E_{pair\ form}/q$, where $E_{pair\ form}$ is the energy of formation of secondary electrons, q is elementary charge. The degree of influence of the potential value of the MCP input electrode on „defocusing" of the electronic pattern of the image of the object and surrounding area is less obvious.

Subject to the foregoing, to study the effect of the potential of the MCP input electrode on the process of pattern formation of images the functional dependences of the average number of photoelectrons projected into the raster of any of the holes of the MCP channels were calculated and graphically presented (Fig. 8). At the same time, the optimal potentials calculated above (1.55, −4.5

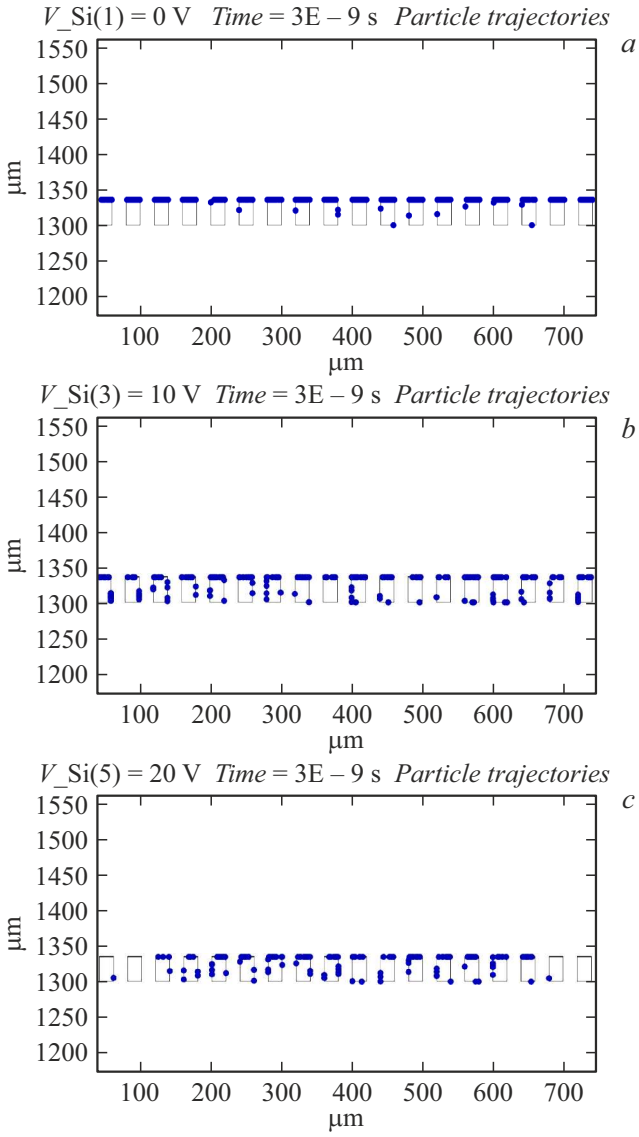

Figure 7. Patterns of photoelectrons (blue dots (in the online version)) captured by the silicon membrane at different potentials on the silicon membrane: *a* — 0, *b* — 10, *c* — 20 V.

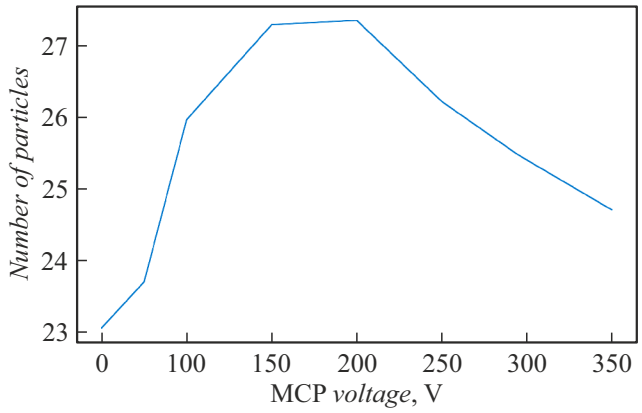

Figure 8. Average number of photoelectrons that reached MCP and projected into the raster of hole of any of its channels vs. potential on MCP input electrode.

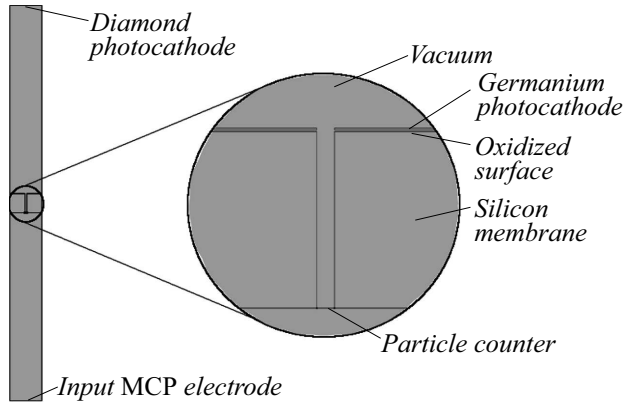

Figure 10. Schematic image of the model representation of the reading unit of image receiver in the form of single-hole membrane used in calculations in the COMSOL Multiphysics software package.

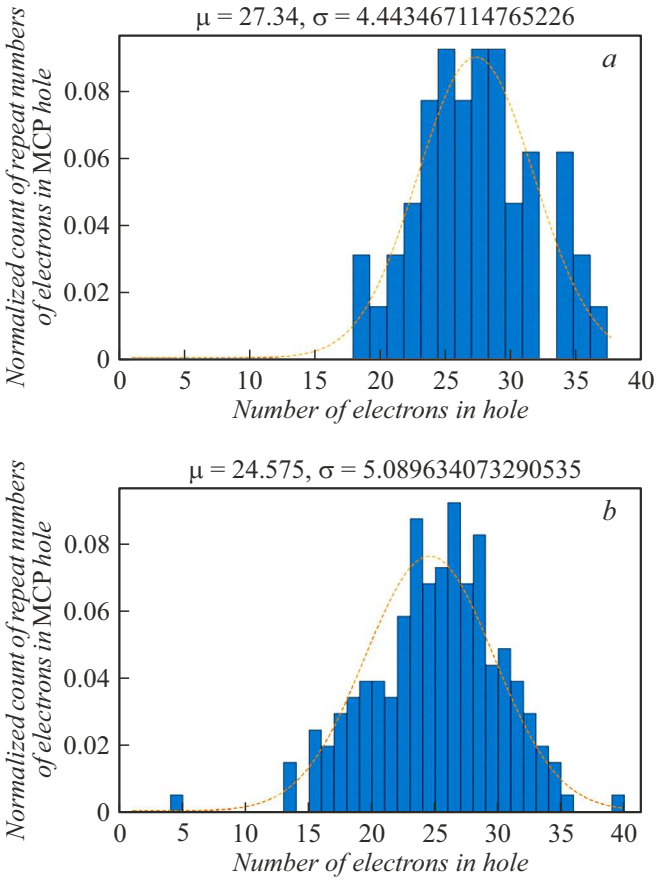

Figure 9. Distribution histograms of the average number of electrons at the input of any of the MCP channels for potentials on the MCP input electrode of 200 (*a*) and 350 V (*b*).

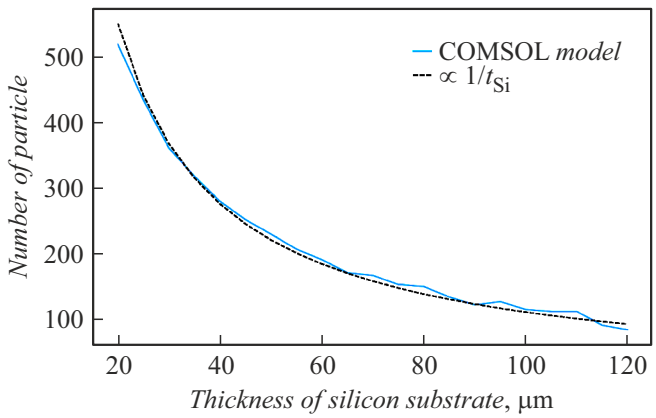

Figure 11. Functional dependence of the number of photoelectrons passing through the silicon membrane on its thickness; the dashed line shows the approximation curve.

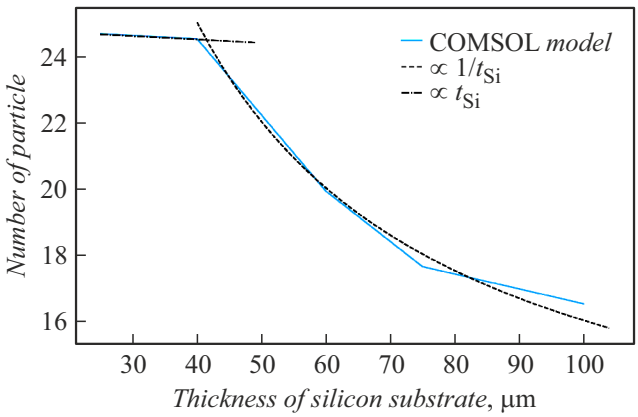

Figure 12. Average number of particles that reached MCP and projected into the raster of the hole of any of its channels vs. silicon membrane thickness.

and −0.45 V, respectively) were set on the device active elements (silicon membrane, diamond and germanium photocathodes), and the potential difference between the MCP electrodes was set by the value ∼ 1000 V.

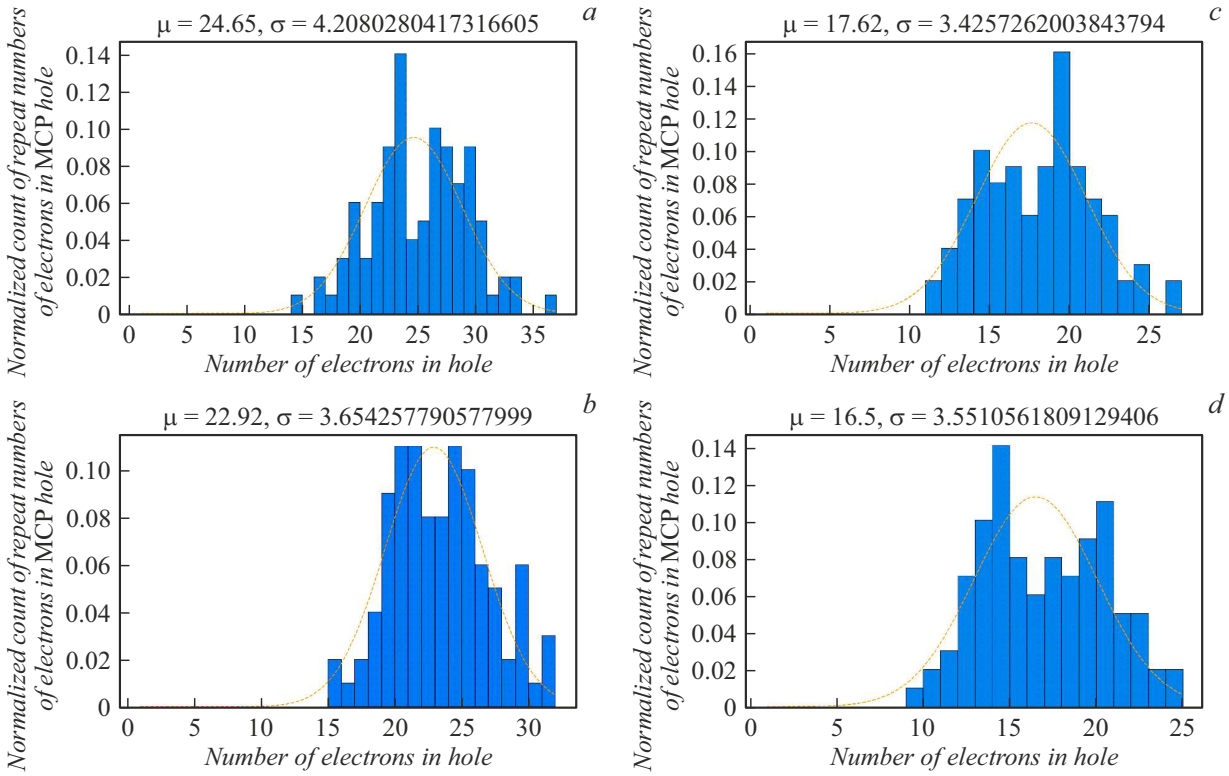

Figure 13. Distribution histograms of the average number of electrons that have reached MCP and projected into the raster of hole of any of its channels, at different thicknesses of the silicon membrane: *a* — 25, *b* — 50, *c* — 75, *d* — 100 μm.

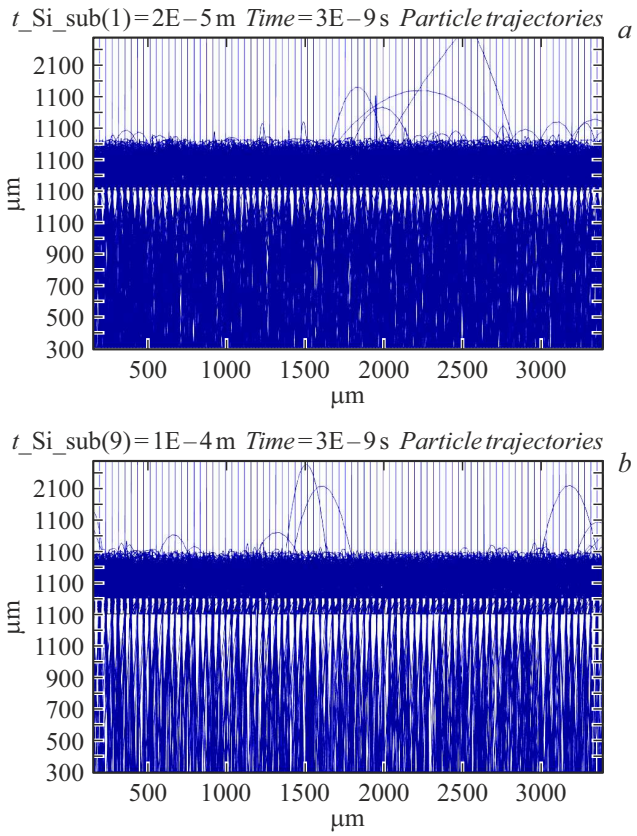

Figure 14. Trajectories of photoelectrons in the vicinity of the surface of the silicon membrane at its various thicknesses: *a* — 20, *b* — 100 μm.

From the numerical calculations presented in Fig. 8 it follows that the optimal value of the potential at the MCP input electrode is $\sim$ 200 V. A further voltage increasing on the MCP input electrode leads to a monotonic decreasing of the average number of electrons entering any of the MCP channels. One of the reasons is the increasing, with increasing of potential, of the fraction of the photoelectrons flow taken away from the channels to the input plane of the MCP, which leads to recombination losses on its surface of a significant part of nonequilibrium electrons. This is confirmed by the distribution histograms of the average number of electrons entering the MCP holes at different potentials at the MCP input electrode (Fig. 9): with an increase in the potential value, the standard deviation increases and the mathematical expectation value decreases. As the analysis of the behavior changes of photoelectron trajectories depending on the voltage at the MPC input electrode shows, another reason for the losses is the „defocusing“ of the photoelectron trajectories of the flow. The dashed line (in Fig. 9) shows the Gaussian distribution by standard deviations and mathematical expectation; the correspondence between the characters of the experimental and Gaussian distributions indicates the random nature of the processes.

1.4. Optimization of silicon membrane thickness

Reducing the thickness of the silicon mesh membrane carrying the germanium photocathode leads to the prob-

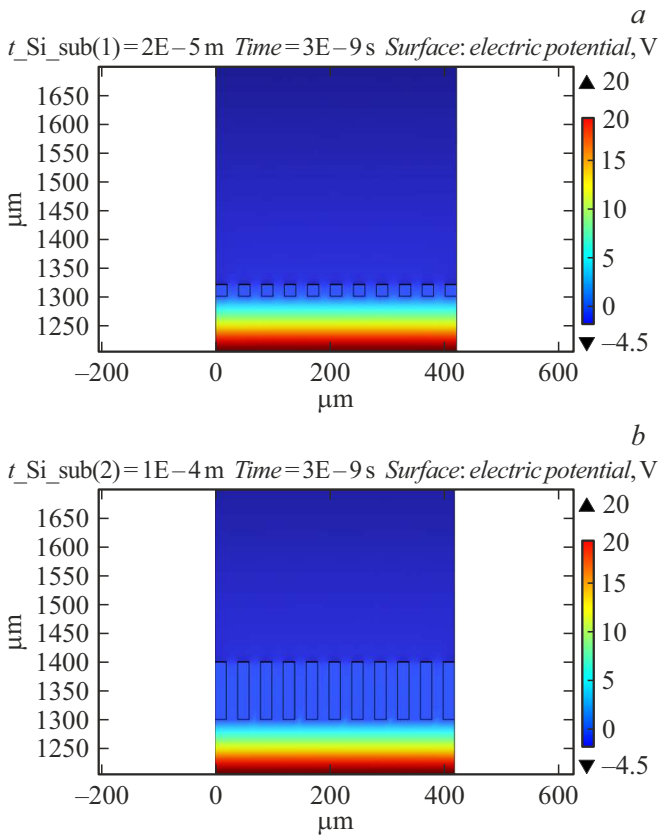

Figure 15. Patterns of the spatial distribution of potentials in the vicinity of the surface of the silicon membrane at its various thicknesses: *a* — 20, *b* — 100 μm.

ability of decreasing electron losses due to their possible collisions with the channel walls and the electrons absorption by the silicon film substance. However, with the thickness decreasing of the silicon mesh membrane, its mechanical strength decreases, and the technical difficulties of its formation increase. It is necessary to keep balance between these factors.

The silicon membrane thickness optimization was carried out using two different approaches. According to one approach (Fig. 2), the operation of the reading unit of the entire multichannel array was simulated. According to the second approach the operation of the reading unit of the image receiver was analyzed by examining any of the holes in the silicon membrane (Fig. 10), which made it possible to significantly improve the statistics of the numerical experiment.

We used models of the reading unit of the membrane with the selection of only one hole to analyze the functional dependence of the number of photoelectrons leaving the silicon membrane depending on its thickness (Fig. 11).

These models, in contrast to those previously described (Fig. 2), make it possible to calculate and graphically represent the functional dependence (Fig. 11) with a larger sample of photoelectrons, which amounted to 2000 photoelectrons produced in the germanium photocathode. The photoelectrons produced by the diamond photocathode slightly perturbed the system and were not considered as quantities of a lower order.

The presented dependence of the number of photoelectrons directed towards the MCP is well approximated by the dependence inversely proportional to the thickness of the silicon membrane. The result obtained was used to refine the functional dependence of the average number of particles reaching MCP and projected onto the area of any of the openings of its channels on the thickness of the silicon membrane (Fig. 12). The results are compared with the results of calculations obtained by us above using other model representations (Fig. 2).

As a result of numerical analysis it was shown (Fig. 12) that the thickness of 40–45 μm can be considered the optimal thickness of the silicon membrane. The resulting functional dependence (dashed curve) is identical to that shown in Fig. 11 for silicon membrane thicknesses over 40 μm.

From the histograms presented in Fig. 13, which describe the distribution of the average number of photoelectrons that fell into the raster of hole of any of the MCP channels

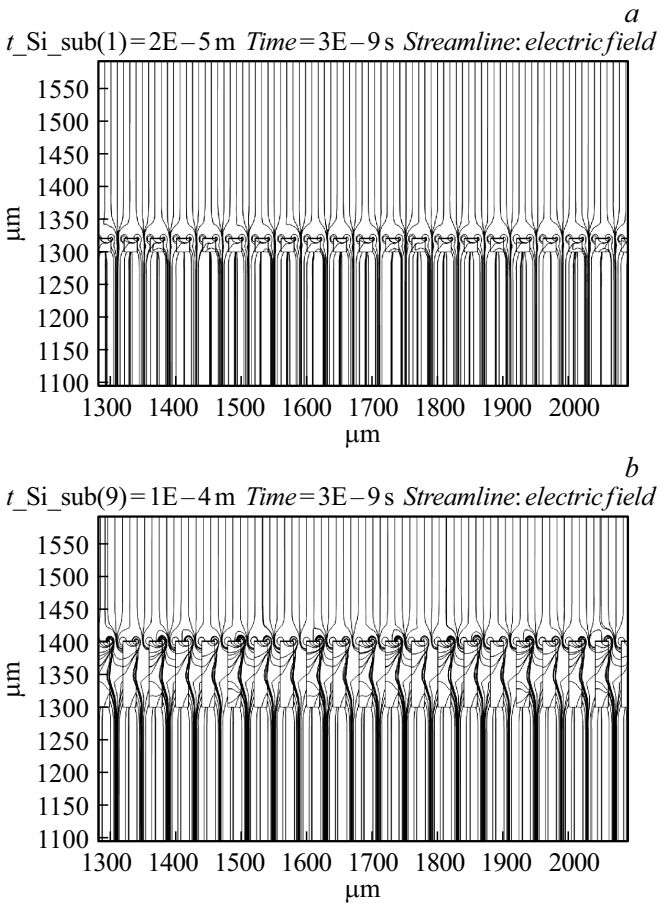

Figure 16. Pattern of the electrical field distribution in the vicinity of the surface of the silicon membrane at its various thicknesses: *a* — 20, *b* — 100 μm.

Basic parameters of the control potentials of the image receiver of objects emitting in the UV range

Potential of silicon membrane, V	Thickness of silicon membrane, μm	Potential on electrode diamond of photocathode, V	Potential on electrode germanium of photocathode, V	Potential on input MCP electrode, V	Potential on output MCP electrode, V	Potential on electrode luminophor, V
1–2	40–45	(−4.5)–(−5)	(−0.45)–(−0.5)	200	1200	2500

depending on the thickness of the silicon membrane, it follows that its thickness increasing leads to decreasing of the number of photoelectrons (decreasing of their mathematical expectation). This can be explained by increasing of the recombination losses of photoelectrons on the channel walls of the silicon membrane, which are not aligned with the channel axes; this is also indicated by the simultaneous decreasing of the root-mean-square deviation. Besides, the thickness decreasing of the silicon membrane leads to an „imbalance" of overlaying of optimal fields in the vicinity of the surface of the germanium photocathode and to „defocusing" of photoelectrons of the resulting flows (Fig. 14, 15). Elimination of the field imbalance by increasing the potential of the MCP input electrode is unacceptable, since this leads to photoelectron losses increasing due to the defocusing of flows in the space silicon membrane –MCP and deviations of part of the flow photoelectrons from the channel raster towards the input MCP plane.

To verify this conclusion, spatial patterns of photoelectron trajectories (Fig. 14) and spatial potential distributions in the vicinity of the silicon membrane (Fig. 15) were plotted.

The facts of the electron losses increasing due to recombination on the channel walls of the membrane with its thickness increasing ($\geq 100\,\mu$m) are clearly manifested in the patterns of the spatial distribution of electric field lines (Fig. 16).

Thus, as a result of numerical calculations and analysis of the results obtained, the optimal values of the potentials of the basic elements of the objects image receiver were selected, they are presented in the Table.

2. Study of the spatial distribution of image patterns of the object and the surrounding area

Below are the results of studies of the integration of one-dimensional models of images patterns of objects and the surrounding area are shown. They are presented in the form of a meander, a sine, and a local object of an arbitrary shape (UV radiation) recorded against the background of constant power radiation from the surrounding area (for example, IR radiation of the night sky reflected from the area). In calculations we used models of the membrane with two hundred (200) holes and a multichannel MCP.

2.1. Signals in the meanders form of meanders (Fig. 17)

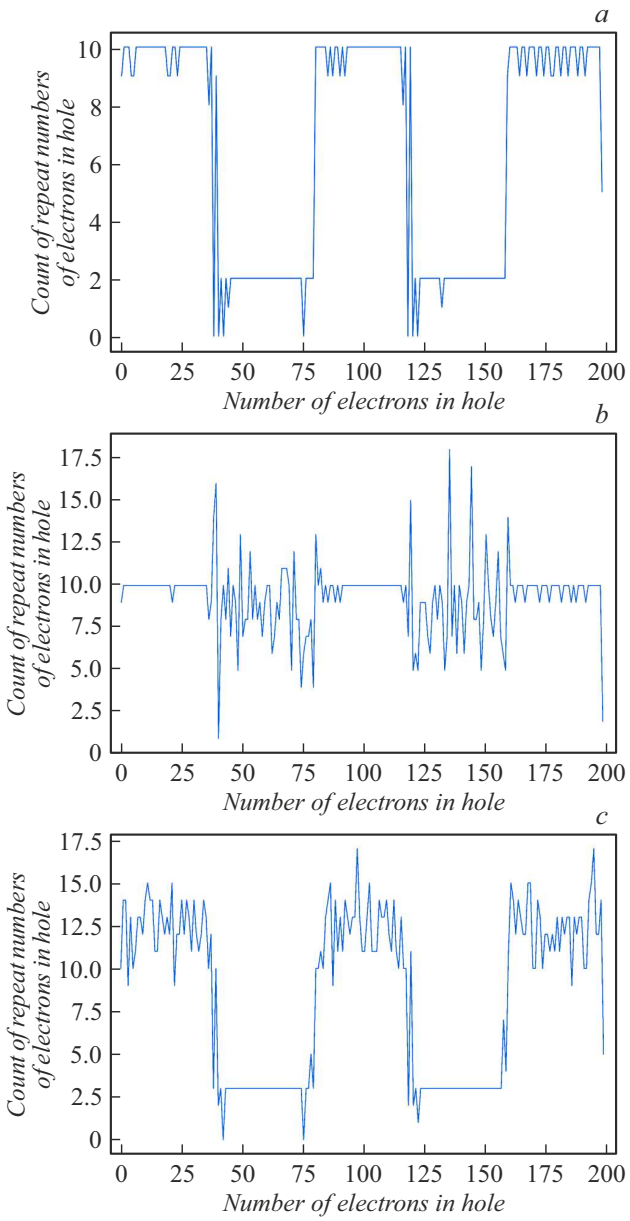

Figure 17. Spatial patterns of images of the object and the surrounding area, taken in the form of a meander: in the absence of IR signal from the surrounding area (a), with signals taken in antiphase (b), with the same phase relations of the signals (c).

2.2. Sine-shaped signals (Fig. 18)

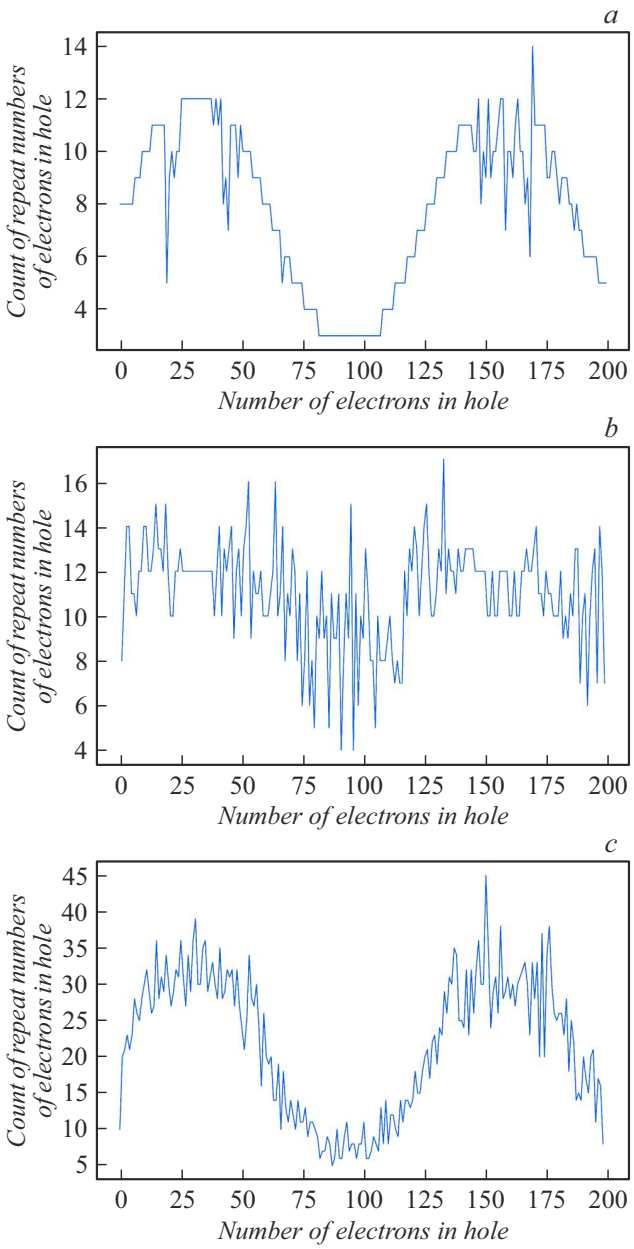

Figure 18. Spatial patterns of the distribution of images of the object and the surrounding area, taken in the form of sines: in the absence of an IR signal from the surrounding area (*a*), in the presence of signals from the object and the area of opposite phases (*b*) and in the presence of signals of the same phases (*c*).

2.3. Registration and recognition of a local UV object against the background of uniform IR flow reflected from the surrounding area (Fig. 19)

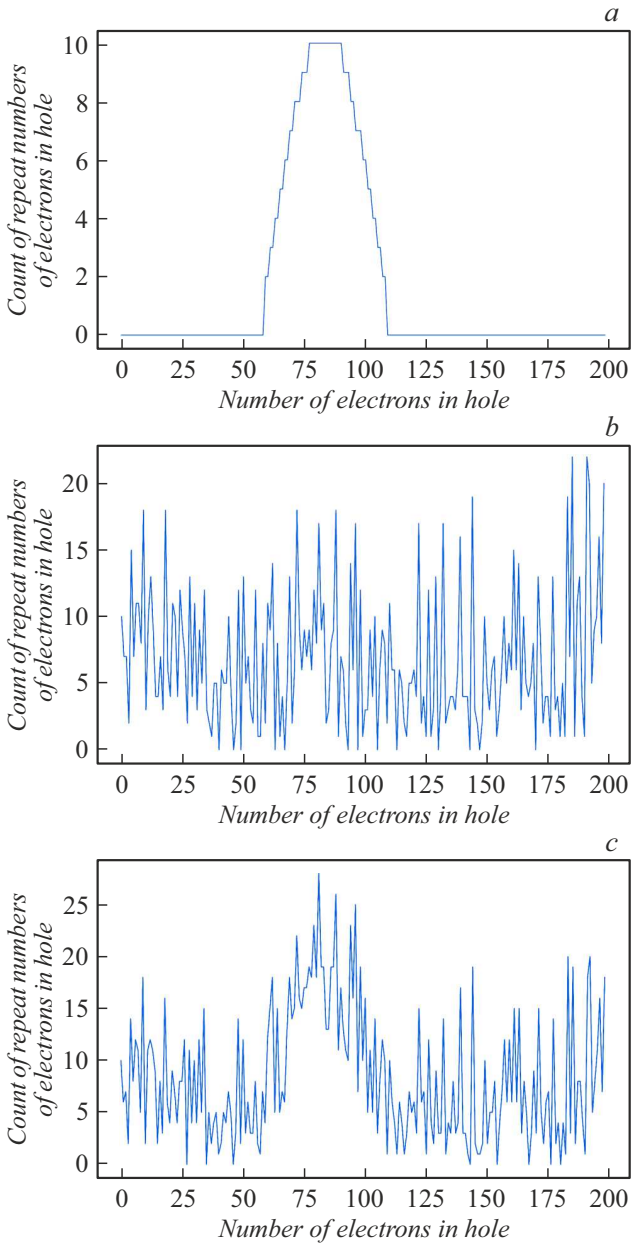

Figure 19. Spatial patterns of the object against the background of the uniform IR radiation flux reflected from the surrounding area: *a* — image of the object; *b* — image of the area, *c* — overlaying of signals from the object and from the area.

Conclusion

A design of single-channel dual-spectrum emission receiver for images of objects emitting in the UV range was suggested, the design implements the object image tie-in to the image of the surrounding area. The images receiver is made in the architecture of the image intensifier tube (IIT); models were formulated, which made it possible to study in detail the processes occurring in its basic units. Using the COMSOL Multiphysics software package, the optimum values of control potentials were calculated, they provide the opportunity of recording and recognizing images of thermal objects in relation to the surrounding area image. The sturdy results will be useful in the development in IIT architecture of innovative single-channel dual-spectrum receiver for images of UV objects in relation to the image of the surrounding area.

Funding

This research was supported financially by the Russian Foundation for Basic Research as part of research project №20-38-90125.

Conflict of interest

The authors declare that they have no conflict of interest.

References

[1] V.A. Bespalov, E.A. Il'ichev, I.P. Kazakov, G.A. Kirpilenko, A.I. Kozlitin, P.V. Minakov, V.V. Saraikin, A.V. Klekovkin, S.V. Kuklev, G.N. Petrukhin, G.S. Rychkov, D.S. Sokolov, E.G. Teverovskaya. Pis'ma v ZhTF, **9**, 3 (2021) (in Russian) DOI: PJTF.2021.09.50897.18480

[2] V.A. Bespalov, E.A. Il'ichev, I.P. Kazakov, G.A. Kirpilenko, A.I. Kozlitin, P.V. Minakov, V.V. Saraikin, A.V. Klekovkin, S.V. Kuklev, G.N. Petrukhin, G.S. Rychkov, D.S. Sokolov, E.G. Teverovskaya. Diamond and Related Mater., **120**, 108603 (2021). DOI: 10.1016/j.diamond.2021.108603

[3] K.N. Mukhin. *Eksperimental'naya yadernaya fizika* (Izd-vo Lan, SPb, 2008), t. 1, s. 297 (in Russian)

[4] L. Feldman, D. Mayer. *Osnovy analiza poverkhnosti i tonkikh plenok* (Mir, M., 1989), s. 49 (in Russian)